HIGH-TEMPERATURE LIQUID-METAL MHD GENERATOR EXPERIMENTS

MASTER

by

P.F. Dunn, E.S. Pierson, J.D. Staffon,

I. Pollack and P.V. Dauzvardis

Prepared for

Eighteenth Symposium

on

Engineering Aspects of MHD

Butte, Montana

18-20 June 1979

NOTICE

[illegible]

ARGONNE NATIONAL LABORATORY, ARGONNE, ILLINOIS

MC-AUA-USDOE

Operated under Contract W-31-109-Eng-38 for the

U. S. DEPARTMENT OF ENERGY

DISTRIBUTION OF THIS DOCUMENT IS UNLIMITED

[illegible]

[illegible]

[illegible]

NOTICE

[illegible]

Presented at the 16th Symposium on Engineering Aspects of Magnetohydrodynamics, 1978

High-Temperature Liquid-Metal MHD Generator Experiments*†

by

P. F. Dunn, E. S. Pierson, J. D. Staffon,
I. Pollack, P. V. Dauzvardis

Argonne National Laboratory
9700 South Cass Avenue
Argonne, Illinois 60439

Abstract

Detailed data were obtained for the world's first high-temperature two-phase liquid-metal MHD generator under open-circuit conditions. Both single-phase (sodium) and two-phase (sodium and nitrogen) flows were used in the temperature range of ~490 to ~740 K. The data presented includes pressures, voltages, and slip ratios (ratio of gas velocity to liquid velocity). The two-phase pressure-gradient data were predicted well by a simplified two-phase MHD correlation that includes the effect of a pure-liquid shunt layer between the electrodes. The slip ratio is shown to decrease with increasing temperature, implying higher generator and system efficiencies; this anticipated result was a prime reason for performing these experiments.

I. Introduction

One of the most critical steps in demonstrating the technical feasibility of the LMMHD (liquid-metal MHD) concept is to test a LMMHD generator at near-actual cycle conditions, in particular, at or near operating temperature. In addition to showing that a high-temperature LMMHD generator can be built and operated successfully, such tests will hopefully verify an anticipated increase in generator performance with increasing temperature (due to a decrease in slip ratio, i.e., the ratio of gas velocity to liquid velocity). The 1978 test results utilizing the world's first experimental high-temperature two-phase LMMHD generator, which was designed, fabricated, and tested at Argonne National Laboratory (ANL), are presented herein.

Detailed data were gathered under open-circuit conditions for both single-phase (sodium) and two-phase (sodium-nitrogen) flows in the temperature range from ~490 to ~740 K. The generator operated at elevated temperatures for a total of 325 hours, including nine complete thermal cycles.

In Section II the facility and generator used for these tests are described briefly. The test conditions and instrumentation are presented in Section III, and the generator pressure gradient and electrode voltage results summarized in Sections IV and V, respectively. The slip ratio findings, which imply an increase in generator efficiency with temperature, are discussed in Section VI.

II. The Facility and Generator

The high-temperature sodium-nitrogen LMMHD facility used for these tests, described elsewhere, provides prescribed flows of liquid sodium [design flow rate of 26 kg/s at 0.79 MPa absolute (115 psia) at 810 K] and gaseous nitrogen [design flow rate of 0.15 kg/s at 1.03 MPa absolute (150 psia) at 810 K] at temperatures from ~480 to ~810 K (~400 to ~1000°F). The sodium and nitrogen are mixed, passed through the test-section (i.e., generator) duct in the presence of transverse magnetic flux densities of up to 0.9 T, and then separated. The sodium is recirculated by an electromagnetic pump, and the nitrogen is vented to the atmosphere after removal of any traces of sodium carryover.

The first experimental high-temperature LMMHD generator, HI-1, the largest generator employed to date in ANL's generator program, is shown in Fig. 1. It was designed to have a power output of approximately 20 kWe, and has approximately a four-times-greater cross-sectional area than previous (ambient-temperature) generators. (For a comparison with other ANL LMMHD generators see (Fig. 1 of the companion LMMHD generator paper.[3]) The generator (Fig. 1) is basically a linearly-tapered, rectangular, thin metal duct, with a 10.2-cm (4.0-in.) uniform electrode spacing and a variable insulating wall spacing of 5.1 to 6.9 cm (2.0 to 2.7 in.). The flow area cross section thus increases along the flow direction so as to maintain a constant liquid velocity of 15.24 m/s (50 ft/s) at the design conditions and, hence, a constant electrode voltage throughout the length of the generator. Because no insulator compatible with high-velocity, high-temperature sodium is readily availalbe, the flow channel walls are fabricated from type 304 stainless steel. The duct wall is made as thin as structurally possible to minimize shorting current losses. The 10.2-cm (4-in.) channel side walls perpendicular to the magnetic field are 0.020 cm (0.008 in.) thick, and are electron beam welded to the 0.051-cm (0.020-in.) thick electrode walls. The heavy copper electrodes are brazed to the latter walls. Structural backup is provided, as shown in Fig. 1.

III. Test Conditions and Instrumentation

The objective of these high-temperature LMMHD generator tests was to establish the baseline performance of the generator over the temperature range of approximately 500 to 800 K. These tests were conducted under open-circuit conditions, i.e., without the generator's load

---

*The submitted manuscript has been authored by a contractor of the U.S. Government under Contract No. W-31-109-ENG-38. Accordingly, the U.S. Government retains a nonexclusive, royalty-free license to publish or reproduce the published form of this contribution, or allow others to do so, for U.S. Government purposes.

†The experimental facility was constructed in part with funds from the Office of Naval Research and the National Science Foundation.

resistors installed. Because of the 0.22-cm conducting walls, this corresponded to a load factor of about 0.97. The primary emphasis was on the investigation of temperature effects, in particular, variations in single-phase and two-phase pressure gradients, voltages, and slip ratios with temperature and other system parameters.

The generator is heavily instrumented for operation and data-acquisition purposes. Thirty-seven system parameters--including conducting walls, this corresponded to a load factor of about 0.97. The primary emphasis was on the investigation of temperature effects, in particular, variations in single-phase and two-phase pressure gradients, voltages, and slip ratios with temperature and other system parameters.

The generator is heavily instrumented for operation and data-acquisition purposes. Thirty-seven system parameters--including temperatures, pressures, flow rates, voltages, magnetic flux density, and void fraction--required for generator performance analysis, in addition to 13 other system monitor parameters, were measured, scanned, and stored by the facility data acquisition system during each experimental run. The pressure difference along the test section was measured with seven pressure transducers spaced along one generator electrode wall. The inlet gas pressure was monitored with an additional pressure transducer, and inlet liquid and gas temperatures by means of thermocouples located between the outer pipe walls and the piping insulation. Mass flow rates and mixture qualities were calculated from the volumetric flow rates measured by the respective liquid (electromagnetic) and gas flowmeters, the pressures, and the temperatures. A transverse magnetic field along 57 cm (22.25 in.) of the approximate center region of the generator was provided by a dc iron-core electromagnet, and the flux density was determined by means of the voltage drop across the calibrated current shunt. Voltages along the positive and negative electrodes were measured by means of five voltage taps along each electrode. Thulium I/O gamma-ray sources were utilized in conjunction with detector/counter instrumentation to determine the void fraction profiles at three stations along the generator axis.

The standard estimates of error for parameter values within the operating range were sodium mass flow rate, 3.1%; nitrogen mass flow rate, 5.1%; temperature, 0.5%; pressure, 3.5%; magnetic flux density, 0.6%; wall voltage, 0.1%; and average void fraction, 13.8%.

A total of 14 single-phase (sodium) and 32 two-phase (sodium-nitrogen) tests were conducted over a range of sodium mass flow rates (14 to 28 kg/s), nitrogen mass flow rates (0 to 0.4 kg/s), average magnetic flux densities (0 to 0.9T), and temperatures (490 to 735 K).

IV. Pressure Measurements

Pressure Profile

The resultant pressure-gradient data for all single-phase flows correlate linearly with the magnetic flux density squared. A typical display of the influence of magnetic flux density, B, on the pressure profile along the generator is shown in Fig. 2 for data obtained at ~620 K. All B = 0 cases examined showed a slight increase in pressure along the generator length, see case 1 of Fig. 2, as expected because the divergence of the channel requires that the velocity decrease. For B ≠ 0, the sharp decrease in pressure near the generator inlet, as compared to the slight decrease or even increase (see Fig. 7 of Ref. 3) near the exit, fig.2, is characteristic of pure-liquid MHD flow in a diverging-area channel. This pressure profile is the result of circulating currents which cause generation near the inlet and pumping near the exit.

A typical display of the influence of magnetic flux density and sodium mass flow rate on the pressure profile for a constant nitrogen mass flow rate is shown in Fig. 3. For lower magnetic flux densities, cases 2 and 5, the generator pressure difference is rather low. As the flux density is increased, cases 3 and 4, the pressure difference becomes larger, but it is still relatively low, as typical for the open-circuit case. Increasing the sodium mass flow rate but maintaining a constant magnetic flux density and nitrogen mass flow rate yields a slight increase in the generator pressure difference, as shown by cases 3 and 4. For constant sodium mass flow rate and temperature, the generator pressure difference increases with increasing average void fraction, as illustrated in Fig. 4. The generator pressure difference was proportional to the square of the magnetic flux density for almost all of the two-phase cases examined.

Two-Phase Correlation

Previous two-phase pressure gradient data gathered at ANL for both circular and rectangular test-section geometries have correlated quite successfully with the predictions of a two-phase MHD pressure-gradient model.[2,4,5] Thus, the model was extended to fit a LMMHD generator with very thin, conducting walls between the electrodes and operated under open-circuit conditions.

For a rectangular generator geometry with the Hartmann number M_{TP}, the model predicts that the two-phase normalized resistance coefficient, λ^*_{TP}, is related to the two-phase Hartmann number, M_{TP}, Reynolds number, Re_{TP}, and conductivity ratio, ϕ_{TP}, by

$$\lambda^*_{TP} = \frac{2\,M_{TP}}{Re_{TP}} \cdot \frac{M_{TP}\,\phi_{TP} + 1}{\phi_{TP} + 1} , \qquad (1)$$

where

$$\lambda^*_{TP} = \lambda_{TP,M} - \lambda_{TP,M=0}$$

$$= \left[\left(-\frac{\Delta p}{\ell}\right)_{TP} \cdot \frac{2d_h}{\rho u^2_{TP}}\right]_M - \left[\left(-\frac{\Delta p}{\ell}\right)_{TP} \cdot \frac{2d_h}{\rho u^2_{TP}}\right]_{M=0} , \qquad (2)$$

$\Delta p/\ell$ is the pressure gradient, ℓ the distance between the first and last pressure transducers (approximately equal to the generator length), and d_h the average channel hydraulic diameter. The values for M_{TP}, Re_{TP}, and ϕ_{TP} are calculated assuming the two-phase liquid velocity given by

$$u_{TP} = u^s/(1 - \bar{\alpha}) \tag{3}$$

and the two-phase conductivity model

$$\sigma_{TP} = \sigma \exp(-3.3\,\bar{\alpha}) \tag{4}$$

of Petrick and Lee[6], where $\bar{\alpha}$ denotes the average void fraction and u^s the superficial liquid velocity. Thus,

$$M_{TP} = B\, d_h \sqrt{\frac{\sigma}{\mu}}\, \exp(-1.9\,\bar{\alpha}) \tag{5}$$

and

$$Re_{TP} = \frac{\rho u^s d_h}{\mu} \cdot \frac{1}{(1-\bar{\alpha})}\,, \tag{6}$$

where B is the average magnetic flux density, and ρ, σ, and μ are the sodium density, electrical conductivity, and absolute viscosity, respectively.

The two-phase conductivity ratio is

$$\phi_{TP} = R_{i,TP}/R_{ext}\,, \tag{7}$$

where

$$R_{i,TP} = \frac{a}{\sigma w \exp(-3.8\,\bar{\alpha})} \tag{8}$$

is the two-phase internal resistance, a the electrode spacing, and w the average channel height parallel to B. The equivalent external resistance, R_{ext}, is the parallel combination of the very thin conducting walls,

$$R_w = \frac{a}{2\ell t \sigma_{sst}}\,, \tag{9}$$

and the liquid-metal shunt layer,[7]

$$R_{sh} = \frac{a}{2\ell\sigma\delta}\,, \tag{10}$$

where σ_{sst} is the stainless steel [illegible], t the conducting wall thickness (0.020 cm), and δ the shunt layer thickness. The shunt layer thickness has been shown by Lykoudis[8] to be

$$\delta = \frac{w}{2} M^{-2/3} \tag{11}$$

Note that w is the upper limit to the shunt layer thickness (it could be less) and that the end resistance R_{end} was not included in R_{ext} as the data fit very well to the theory. The contribution of R_{end} is less than the uncertainly in R_{sh}.

The two-phase normalized resistance coefficients from the pressure-gradient data are compared with the theoretical predictions in Fig. 5. The least-squares fit of the data agreed quite well with the theoretical prediction, to within 20% (correlation coefficient = 0.85, standard error of estimate = 0.09).

V. Voltages

For all single-phase cases examined, the electrode voltages were predominantly proportional to the magnetic flux density at each voltage tap location. The voltage profiles did exhibit, however, a characteristic asymmetry due to the velocity decrease along the divergent channel, as shown in Figs. 6 and 7. When the sodium mass flow rate, hence average liquid velocity, was decreased, the electrode voltages decreased. This difference is displayed between Figs. 6 and 7 in which the sodium mass flow rates were approximately 28.0 and 14.4 kg/s.

The characteristic shape of the electrode voltage profile obtained for two-phase flows is shown in Fig. 8. For those cases examined which were close to design conditions, the voltage potential along the electrodes was almost constant, implying that the generator was designed properly for two-phase operation. The slight decrease along the channel occurred because the generator was not loaded as designed, thus the gas expansion was less than expected and the liquid velocity decreased along the generator.

VI. Slip Ratios

A significant decrease in two-phase EMMHD generator and cycle efficiencies occurs when the gas travels faster than the liquid metal in the generator, thereby increasing the losses and decreasing the interfacial energy transfer. The ANL ambient-temperature generator experiments have shown that the average slip ratio (average ratio of gas velocity to liquid velocity), $\bar{K}$, decreases and approaches unity with increasing liquid-metal flowrate,[3] as anticipated. The anticipated decrease in $\bar{K}$ with increasing temperature (due to changes in the liquid properties, e.g., surface tension), had not previously been demonstrated; its demonstration was a prime motivation for these high-temperature experiments.[9]

The variation in $\bar{K}$ with temperature is best observed by comparing values at the same gas-to liquid volume ratio. Using the definitions of the two-phase mixture average hold-up (ratio of gas-to-total volume flow rates) and the average void fraction (ratio of gas-to-total flow cross-sectional areas), $\bar{\alpha}$, the relation

$$\frac{\bar{\alpha}}{1-\bar{\alpha}} = \frac{1}{\bar{K}}\,\frac{\beta}{1-\bar{\beta}} \tag{12}$$

can be derived, where β (β) is the ratio of gas to liquid volume flow rates and $\bar{\alpha}/(1-\bar{\alpha})$ is the ratio of gas-to liquid flow cross-sectional areas. Equation (12) indicates that as $\bar{K}$ approaches unity a larger ratio of gas-to-liquid flow cross-sectional areas, i.e., larger $\bar{\alpha}/(1-\bar{\alpha})$ values are achieved for the same ratio of gas-to liquid volume flow rates, i.e., more of the channel is filled with gas.

The values of $\bar{\beta}/(1-\bar{\beta})$ and $\bar{\alpha}/(1-\bar{\alpha})$ for all two-phase data obtained at temperatures of 520 K and 660 K and B from 0.3 T to 0.9 T are plotted in Fig. 9. A significant decrease in $\bar{K}$ is observed for the higher temperature, as anticipated, particularly for the larger values of

$\bar{\beta}/(1-\bar{\beta})$. (A decrease in R is shown by a higher $\bar{\alpha}/(1-\bar{\alpha})$ value for the same $\bar{\beta}/(1-\bar{\beta})$ value.) Also noticeable are values of R close to unity for the higher liquid-metal flow rates, i.e., lower $\bar{\beta}/(1-\bar{\beta})$ values.

VII. Conclusions

The experimental data from the first high-temperature two-phase LMMHD generator have demonstrated the desired result, a reduction in the ratio of the gas velocity to the liquid velocity with increasing temperature. This information, when combined with the positive findings in the companion ambient-temperature generator paper,[3] provide convincing evidence that large, high-efficiency two-phase LMMHD generators can be developed for practical power systems.

NOMENCLATURE

a	electrode spacing
B	average magnetic flux density
d_h	average channel hydraulic diameter, $2aw/(a+w)$
R	average slip ratio
ℓ	length between first and last generator pressure transducers
$\dot{m}_g$	gas mass flow rate
$\dot{m}_\ell$	liquid mass flow rate
M	Hartmann number, $Ba\sqrt{\sigma/\mu}$
p	pressure
Q	volumetric flow rate
Re	Reynolds number, $\rho u d/\mu$
R_{ext}	equivalent external resistance
R_i	internal generator resistance, $a/2w\sigma$
R_{sh}	shunt layer resistance, $a/2\delta\sigma$
R_w	wall resistance, $a/2\sigma_{sst}t$
t	thickness of wall between generator electrodes
T	temperature
u	velocity
u^s	superficial liquid velocity, $\dot{m}_\ell/\rho wa$
w	average channel height parallel to B
$\bar{\alpha}$	average void fraction, $\dot{m}_g\rho_\ell/(\dot{m}_g\rho_\ell + K\dot{m}_\ell\rho_g)$
$\bar{\beta}$	average hold-up, $Q_g/(Q_g + Q_\ell)$
δ	shunt layer thickness
δp	pressure difference between first and last generator transducers
λ_*	resistance coefficient, $(-\Delta p/\ell)\cdot(2d/\rho u^2)$
λ^*	normalized resistance coefficient, $\lambda_M - \lambda_{M=0}$
μ	absolute viscosity of sodium
ρ	density of sodium
σ	electrical conductivity of sodium
σ_{sst}	electrical conductivity of stainless steel
ϕ	conductivity ratio, R_i/R_{ext}

Subscripts

g	gas
ℓ	liquid
SP	single phase
sst	stainless steel
TP	two phase

Acronyms

ANL	Argonne National Laboratory
LMMHD	Liquid Metal Magnetohydrodynamic

References

1. System Design Description, High Temperature Liquid-Metal MHD Facility, ENG Div. Doc. No. G0017-0157-SA-01, Budget Act. No. 49725, Argonne National Laboratory, 1977.

2. Pierson, E. S., Dauzvardis, P. V., and Dunn, P. F., "Sodium-Nitrogen Liquid-Metal MHD Facility Initial Test Results", Proc. of the 16th Symp. on Engrg. Aspects of MHD, Philadelphia, PA, 1976.

3. Fabris, G., Pierson, E. S., Pollack, I., Dauzvardis, P. V., and Ellis, W., "High-Power-Density Liquid-Metal MHD Generator Results", Proc. of the 16th Symp. on Engrg. Aspects of MHD, Butte, MT, 1979.

4. Dunn, P. F., Fabris, G., Pierson, E. S., and Petrick, M., Two-Phase Liquid-Metal MHD Generator Experiments and Pressure-Gradient Correlations. Second Bat-Sheva Seminar on MHD Flows and Turbulence, 1978, Beer-Sheva, Israel.

5. Dunn, P. F., Single and Two-Phase Magnetohydrodynamic Pipe Flow, submitted to the International Journal of Heat and Mass Transfer, September, 1978.

6. Petrick, M. and Lee, K. Y., 1964 Performance characteristics of a liquid metal MHD generator. Proc. Symp. on MHD Elec. Power Gen., 2, 953-970.

7. Dunn, P. F., LMMHD Generators, pp. 78-94, Proceedings of the Rand Corporation Conference on Liquid-Metal MHD Power Generation, Pei, R. Y., and Purnell, S. W., Eds., R-2290-DOE, 1978.

8. Lykoudis, P. S., Shunt Layer Thickness, Argonne National Laboratory LMMHD Group Memo 77-2, 1977.

9. Plan for Determining the Characteristics of the High-Temperature Liquid-Metal MHD Generator, Budget Act. No. 49725, Argonne National Laboratory, 1977.

Case	Symbol	B (T)	$\dot{m}_\ell$ (kg/s)
1	□	0	27.87
2	○	0.65	28.06
3	△	0.80	27.69
4	+	0.91	26.08
5	×	0.91	14.43

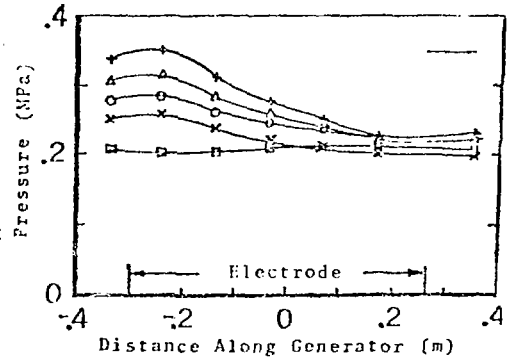

Figure 2
Single-Phase Sodium Pressure Profile Data, T ≅ 620 K

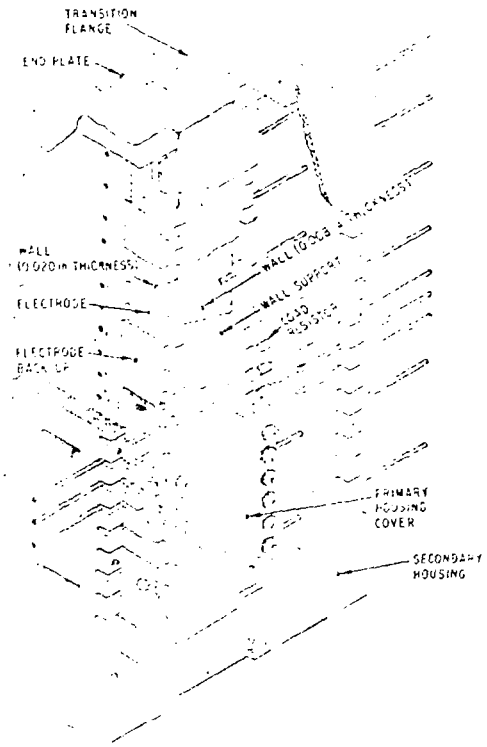

Figure 1
Cutaway View of AGL LMMHD Generator MT-1

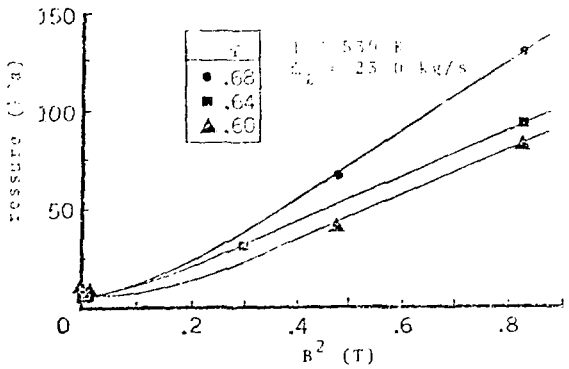

Figure 2
Two-Phase Sodium-Nitrogen Generator Pressure Difference Versus Average Magnetic Flux Density Squared, T ≅ 530 K

Case	Symbol	B (T)	$\dot{m}_l$ (kg/s)	$\dot{m}_g$ (kg/s)
1	□	0	23.83	0.200
2	○	0.55	22.55	0.201
3	△	0.91	18.60	0.200
4	+	0.91	24.30	0.191
5	×	0.57	28.07	[illegible]

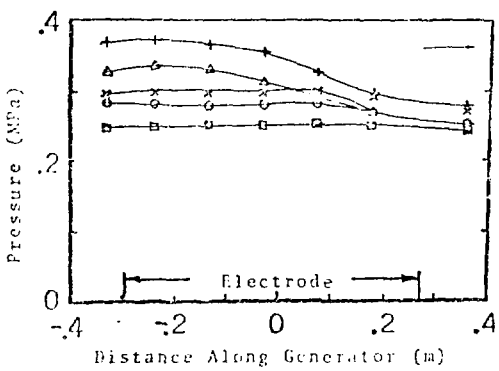

Figure 3
Two-Phase Sodium-Nitrogen Pressure Profile Data, T ≅ 540 K

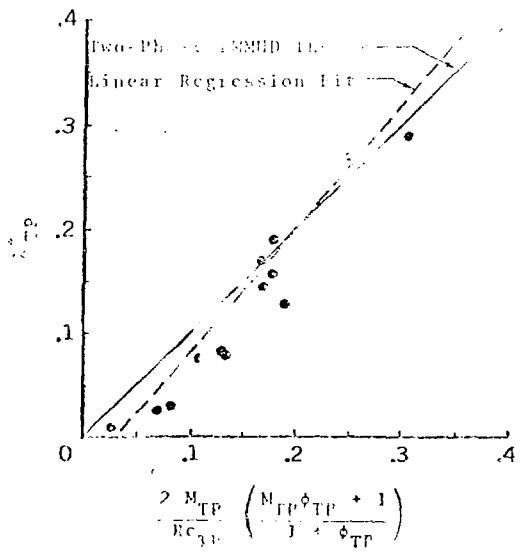

Figure 5
Two-Phase Normalized Resistance Coefficient Comparison with Theory, T ≅ 500 K to T ≅ 675 K

Case	Symbol	B (T)	$\dot{m}_\ell$ (kg/s)
1	□	0	27.87
2	○	0.65	28.06
3	△	0.80	27.69
4	+	0.91	28.08
5	×	0.91	14.43

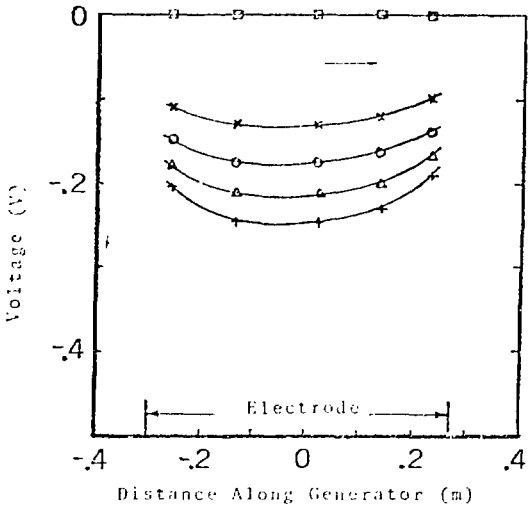

Figure 6
Single-Phase Sodium Generator Negative Electrode Profile Data, T ≅ 730 K

Case	Symbol	B (T)	$\dot{m}_\ell$ (kg/s)	$\dot{m}_g$ (kg/s)
6	□	0.69	28.12	0.094
7	○	0.25	28.09	0.090
8	△	0	27.75	0.090
10	×	0.26	22.28	0.347

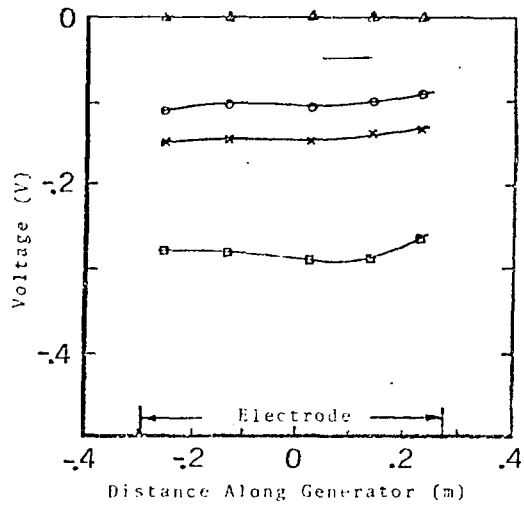

Figure 8
Two-Phase Sodium-Nitrogen Generator Negative Electrode Profile Data, T ≅ 525 K

Case	Symbol	B (T)	$\dot{m}_\ell$ (kg/s)
2	□	0	14.25
3	×	0.35	14.31
4	+	0.65	14.46
5	△	0.80	14.50
6	○	0.91	14.55

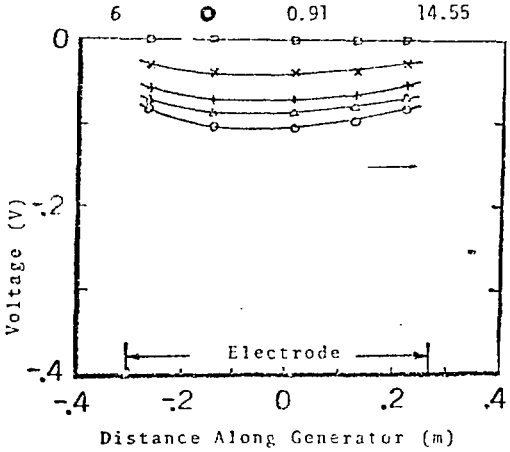

Figure 7
Single-Phase Sodium Generator Negative Electrode Profile Data, T ≅ 620 K

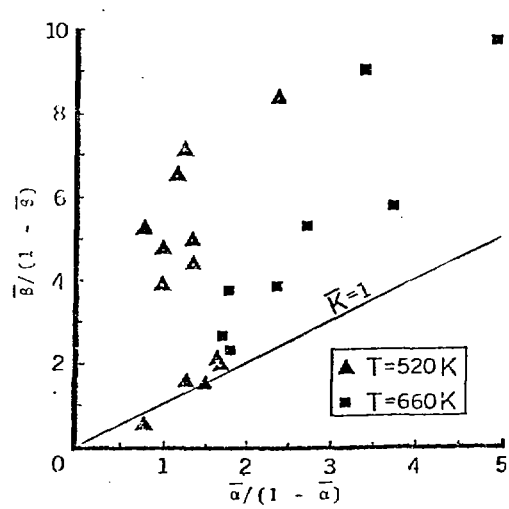

Figure 9
Influence of Temperature on the Generator Average Slip Ratio, T ≅ 520 K and T ≅ 660 K